

NUMERICAL MODELING OF THE STRESS-STRAIN RESPONSE IN PROGRESSIVE LOADING CYCLES OF POLYESTER MULTIFILAMENTS

Daniel Magalhães da Cruz[1] - daniel.cruz@ufrgs.br
Tales Luiz Popiolek Júnior[2] - talespopiolekjr@furg.br
Ivan Napoleão Bastos[3] - inbastos@iprj.uerj.br
Adilson Pinto da Silva[3] - adilson.silva@iprj.uerj.br
Ana Lúcia Nazareth da Silva[4] - ananazareth@ima.ufrj.br
Jakson Manfredini Vassoler[1] - jmvassoler@ufrgs.br
Felipe Tempel Stumpf[1] - felipe.stumpf@ufrgs.br
[1]Federal University of Rio Grande do Sul (UFRGS) - Porto Alegre - RS - Brazil
[2]Federal University of Rio Grande (FURG) - Rio Grande - RS - Brazil
[3]Rio de Janeiro State University (UERJ) - Nova Friburgo - RJ - Brazil
[4]Federal University of Rio de Janeiro (UFRJ) - Rio de Janeiro - RJ - Brazil

Abstract. *This work presents a numerical approach to simulate the stress-strain behavior of polyester multifilaments subjected to progressive tension dynamic cycles with increasing load amplitudes up to* 50% *of the Yarn Break Load (YBL). A phenomenological hyperelastic model (Modified Yeoh) was implemented using a tensorial formulation grounded in continuum mechanics and calibrated via parametric optimization. Experimental cyclic loading data at* 0.1 *Hz with sinusoidal waveforms force-controlled were used to validate the numerical model. The simulations captured the constitutive response at varying load levels with satisfactory accuracy, even under non-stabilized hysteresis conditions. Results indicated that while the average simulation error varied across cycles, the methodology consistently reproduced the mechanical behavior of polyester multifilaments. The largest amplitude cycle (*0 *to* 50%*YBL) showed the closest visual agreement between numerical and experimental curves (and similar loading-unloading), whereas the* 0 *to* 20%*YBL cycle presented the lowest quantitative error. Numerical parameters remained consistent throughout the cycles, demonstrating the robustness of the implemented code. These findings support the potential of the proposed method for extending constitutive simulations to higher structural levels such as strands and sub-ropes. Future work should investigate the effects of frequency, loading rates, and hysteresis stabilization, and include testing other synthetic fibers and single-cycle loading.*

Keywords: *Constitutive simulation, Dynamic loading, Mechanical hysteresis, Synthetic yarns, Polyester fibers*

1. INTRODUCTION

In recent decades, synthetic fibers have revolutionized materials engineering, playing a prominent role in various structural applications due to their high specific strength, low weight, flexibility, mechanical properties, and resistance to environmental degradation (Bhat, 2017; Ahmad et al., 2020). In the offshore context, these materials have gained particular relevance as mooring lines, emerging as alternatives to traditional steel catenary systems and enabling new anchoring concepts in taut-leg configurations using synthetic fiber ropes (Del Vecchio, 1992; Banfield and Casey, 1998; Lee et al., 1999). Among the most prominent polymeric fibers, polyester (polyethylene terephthalate, PET) has become one of the most widely used options, offering reliable mechanical performance, environmental stability, and cost-effectiveness (Bastos, 2013; Bastos et al., 2016).

The progressive replacement of steel cables with synthetic fibers in offshore mooring lines has fostered the development of a robust research field, with growing interest in the multiscale understanding of the mechanical behavior of these fibers (Weller et al., 2015; Bastos and da Silva, 2020; da Cruz et al., 2024c). In parallel, the advancement of experimental, analytical, and especially numerical methodologies for evaluating these fibers has progressed significantly. Among these approaches, constitutive numerical simulation stands out for its ability to represent, with a good degree of accuracy and low computational cost, the stress-strain behavior of polymeric materials under different loading conditions.

In this context, the present work is part of a consolidated research line focused on the constitutive numerical simulation of the mechanical behavior of synthetic fibers, based on phenomenological strain energy models derived from nonlinear elasticity theory and continuum mechanics (da Cruz, 2022). The numerical code used was developed in Matlab, based on the formulation by Simo and Hughes (2006), and has been applied in various studies by the research group, involving the simulation of mechanical hysteresis, fatigue, creep, and tensile failure in multifilaments, subropes, and hybrid configurations of synthetic fibers (da Cruz et al., 2023; Stumpf et al., 2023, 2024; da Cruz et al., 2024a,b).

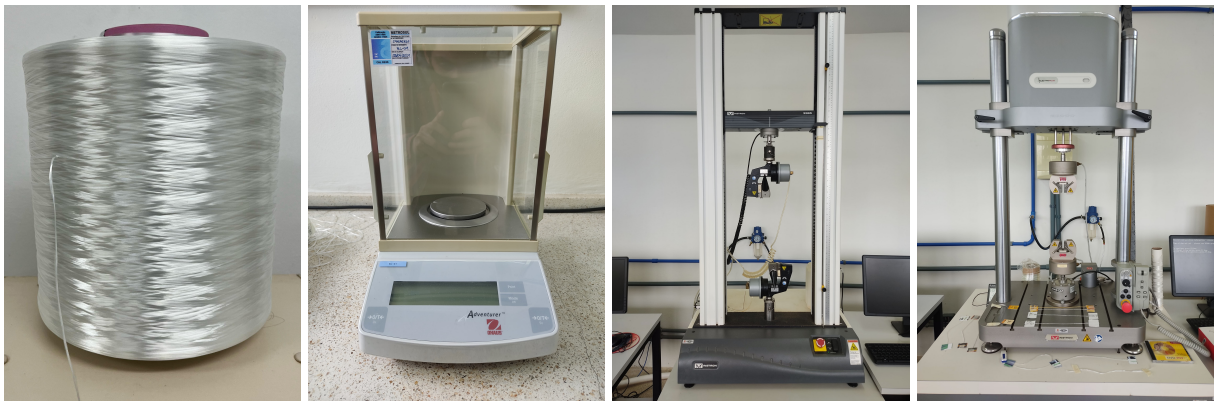
Although several studies have analyzed the constitutive behavior of polyester fibers under mechanical hysteresis, the stress-strain response of polyester multifilaments under varying dynamic load amplitudes has not yet been numerically explored. Likewise, the direct influence of maximum load levels on hysteresis has not been investigated without considering cycle accumulation or hysteresis stabilization. Therefore, this work aims to fill this gap by investigating, for the first time, the constitutive simulation of five consecutive (non-stabilized) zero-to-tension loading cycles with increasing amplitudes: from 0 to 10%, 0 to 20%, 0 to 30%, 0 to 40%, and 0 to 50% of the Yarn Break Load (YBL). The experimental tests were conducted at a frequency of 0.1 Hz with a sinusoidal waveform, and the experimental response was used as a reference for numerical calibration.

The central objective of this study is to evaluate the predictive capability of a constitutive model (phenomenological strain energy function), calibrated via parametric optimization with experimental data, to represent the mechanical response of polyester under this progressive loading protocol. The proposed analysis aims not only to assess the accuracy of the simulation under non-stabilized conditions but also to explore the evolution of hysteresis and stiffness with increasing load amplitude, providing new insights for the mechanical modeling of synthetic fibers in offshore applications. Furthermore, this study seeks to lay the groundwork for the development of more comprehensive predictive models and to advance these investigations to higher structural levels, such as strands and subropes.

2. MATERIALS AND METHODS

2.1 Initial Fiber Characterization

The fiber under investigation is polyester (polyethylene terephthalate, PET) in the form of multifilaments, specifically designed for the fabrication of offshore mooring ropes or nautical ropes. The samples were extracted from a virgin spool of untwisted multifilaments (Fig. 1a). Several tests were performed for the initial characterization of fiber: linear density, Yarn Break Load (YBL), and linear tenacity. All tests were conducted under temperature and humidity conditions compliant with ISO 139 (International Organization for Standardization, 2005).



(a) Untwisted PET spool (b) Precision Balance (c) Instron 3365 (d) Instron E3000

Figure 1: Material and equipment.

The linear density of the material (ρ_L) is determined with a series of mass-per-length measurements, following ASTM D1577 (American Society for Testing and Materials, 2018). Fifteen specimens with a standard length of 1000 millimeters were used. After a stabilization period of 9 minutes, the mass was measured using a precision balance (Fig. 1b), with the linear density expressed as tex [g/km].

The rupture test (YBL) was conducted in accordance with ISO 2062 (International Organization for Standardization, 2009), using a universal testing machine (Fig. 1c). A total of 15 specimens were tested, each with a standard length of 1000 mm and a twist of 60 turns per meter. Once fixed on the equipment, the effective gauge length was 500 mm. The test was performed at a constant extension rate of 250 mm/min. The data acquired during the test are force [N] and extension [mm].

The linear tenacity (T_L) of the material is determined by averaging the obtained results, calculated by dividing the tensile strength by the linear density, yielding the linear tenacity expressed in [N/tex]. According to ISO 18692-2 (International Organization for Standardization, 2019), this value must be at least 0.78 N/tex for polyester multifilaments intended for mooring ropes.

Table 1 presents the results of the initial characterization in terms of linear density (ρ_L), rupture force (F_{rup}), rupture stress (σ_{rup}), rupture strain (ε_{rup}), and linear tenacity (T_L), as well as the fiber's specific mass (ρ), which is provided by the manufacturer and also reported in previous literature (Weller et al., 2015; da Cruz et al., 2025).

As shown in Table 1, a rupture stress estimate is provided, which is essential for the numerical code, as dimensional consistency is required for the experimental data used in the

Table 1: Experimental results for initial mechanical characterization

ρ_L [tex]	F_{rup} [N]	σ_{rup} [MPa]	ε_{rup} [%]	T_L [N/tex]	ρ [g/cm^3]
223.04	178.58	1104.92	12.13	0.801	1.38

calibration process. The classical definition of stress as the ratio between force and cross-sectional area is difficult to apply in this case due to the lack of precision in determining the area of a bundle of filaments. To address this limitation, an alternative mathematical approach is adopted, in which stress (σ) in mega Pascals is calculated based on force (F) in Newtons, linear density (ρ_L) in grams per meter, and specific mass (ρ) of the material in grams per cubic centimeter, as shown in Eq. (1). The units indicated ensure the correct adjustment of the Eq. (1).

$$\sigma = \frac{F \times \rho}{\rho_L} \tag{1}$$

2.2 Experimental Simple Progressive Cycles

The dynamic cycles numerically simulated in this study, calibrated using experimental data, consist of zero-to-tension cycling controlled by load, with a sinusoidal waveform and a frequency of 0.1 Hz. The tests were conducted progressively with respect to load amplitude, comprising five consecutive cycles: from 0 to 10%, 0 to 20%, 0 to 30%, 0 to 40%, and 0 to 50% of the YBL, totaling a test duration of 50 seconds. Figure 2 schematically illustrates the loading protocol. It is important to note that the tests were conducted under controlled temperature and humidity conditions, in accordance with ISO 139 (International Organization for Standardization, 2005).

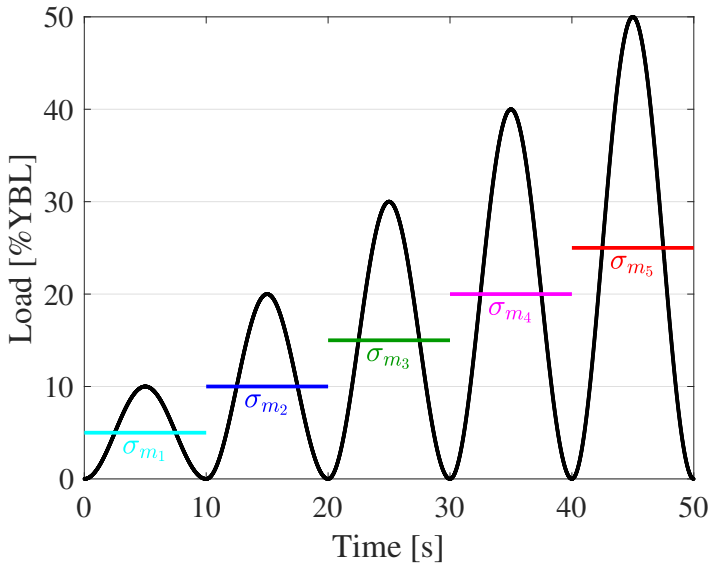


Figure 2: Schematic of the experimental simple progressive cycles.

Although the stress ratio (R), defined as the minimum stress divided by the maximum stress, remains zero for the variable amplitude loading used in this study, the mean stress (σ_m) progressively increases, as indicated by the colored curves in Fig. 2. The stress exhibits a tensile characteristic for all the tests.

2.3 Numerical Development

The numerical simulations will be performed individually for each dynamic cycle obtained (single, not grouped curves). Therefore the numerical methodology will be executed for 5 dynamic conditions, respective to the load amplitudes: 0 to 10%, 0 to 20%, 0 to 30%, 0 to 40%, and 0 to 50% of the YBL.

The numerical implementation adopted in this study is based on the finite deformation formulation described by Simo and Hughes (2006), and on subsequent developments applied to synthetic fibers by da Cruz (2022). The simulations were implemented in MATLAB and are grounded in elasticity theory, continuum mechanics, properties of the polymeric material, and hyperelastic behavior.

Let $\Omega \subset \mathbb{R}^3$ be a body subjected to finite deformation $\varphi : \Omega \to \mathbb{R}^3$. The deformation gradient is defined as $\mathbf{F} = \partial\varphi\left(\mathbf{X}\right)/\partial\mathbf{X}$, where $\mathbf{X}$ denotes a point in the reference configuration (undeformed). The Jacobian is $J = \det \mathbf{F} > 0$.

The deformation gradient ($\mathbf{F}$) can be multiplicatively decomposed into a volumetric part ($\hat{\mathbf{F}}$) and an isochoric part ($\bar{\mathbf{F}}$), following the classical Flory decomposition (Flory, 1961), shown in Eq. (2), Eq. (3) and Eq. (4) and where $\mathbf{I}$ corresponds to a unitary identity matrix.

$$\mathbf{F} = \hat{\mathbf{F}}\,\bar{\mathbf{F}} \tag{2}$$

$$\hat{\mathbf{F}} = J^{1/3}\mathbf{I}, \quad \text{with} \quad \det\hat{\mathbf{F}} = J \tag{3}$$

$$\bar{\mathbf{F}} = J^{-1/3}\mathbf{F}, \quad \text{with} \quad \det\bar{\mathbf{F}} = 1 \tag{4}$$

A deformable body stores mechanical energy in the form of strain energy. This is represented by a strain energy density function (W). For hyperelastic materials, this function can be additively split into volumetric (W^{vol}) and isochoric (W^{iso}) components, as shown in Eq. (5), and in the case of incompressible or nearly incompressible materials (which is the case with synthetic fibers), the volumetric contribution W^{vol} is negligible or vanishes entirely, allowing the formulation to focus on the isochoric component W^{iso}, as expressed in Eq. (6).

$$W(\mathbf{C}) = W^{\text{vol}} + W^{\text{iso}} \tag{5}$$

$$W(\bar{\mathbf{C}}) = W^{\text{iso}} \tag{6}$$

This decomposition is essential for developing the stress tensors in purely isochoric terms, which aligns with the constitutive modeling of polymeric materials. Thus, the isochoric right Cauchy-Green deformation tensor $\bar{\mathbf{C}}$ is given in Eq. (7). And the invariants of continuum mechanics with respect to the right Cauchy-Green tensor ($\bar{\mathbf{C}}$) are defined in Eq. (8) for the first invariant, in Eq. (9) for the second invariant, and in Eq. (10) for the third invariant.

$$\bar{\mathbf{C}} = \bar{\mathbf{F}}^T\bar{\mathbf{F}} = J^{-2/3}\mathbf{C}, \quad \text{where} \quad \mathbf{C} = \mathbf{F}^T\mathbf{F} \tag{7}$$

$$\bar{I}_1 = \operatorname{tr}\bar{\mathbf{C}} \tag{8}$$

$$\bar{I}_2 = \frac{1}{2}\left[\left(\operatorname{tr}\bar{\mathbf{C}}\right)^2 - \operatorname{tr}\left(\bar{\mathbf{C}}^2\right)\right] \tag{9}$$

$$\bar{I}_3 = \det\bar{\mathbf{C}} = 1, \quad \text{incompressible} \tag{10}$$

An internal variable ($\mathbf{H}$), shown in Eq. (11), is introduced to account for material memory effects, and it is updated at each time step (Δt_n) as a function of the material relaxation (τ_i) and the Piola-Kirchhoff stress in isochoric term ($\bar{\mathbf{S}}$). This stress tensor in isochoric terms ($\bar{\mathbf{S}}$) is also

presented in Eq. (12), note its dependence on the isochoric Cauchy-Green deformation tensor ($\bar{\mathbf{C}}$), and also the appearance of the strain energy function (W).

$$\mathbf{H}_{n+1} = e^{-\Delta t_n/\tau_i}\,\mathbf{H}_n + e^{-\Delta t_n/(2\tau_i)}\left(\bar{\mathbf{S}}_{n+1} - \bar{\mathbf{S}}_n\right) \tag{11}$$

$$\bar{\mathbf{S}} = 2\left(\frac{\partial W}{\partial I_1} + \frac{\partial W}{\partial I_2}\right)\mathbf{I} - 2\,\frac{\partial W}{\partial I_2}\,\bar{\mathbf{C}} + 2\,\frac{\partial W}{\partial I_3}\,I_3\,\bar{\mathbf{C}}^{-1} \tag{12}$$

Within the development of the numerical code an incremental deformation matrix is defined. This allows calculating the left ($\mathbf{B}$) and right ($\mathbf{C}$) Cauchy-Green strain tensors, operating with the strain matrix ($\mathbf{F}$) and its transposition according to continuum mechanics.

Deviatoric functions are calculated for the second Piola-Kirchhoff stress tensor ($\mathbf{S}$) and for the internal variable ($\mathbf{H}$). Equation (13) shows the mathematical formulation used to compute this deviatoric function. The superscript "$\circ$" indicates the application of the deviatoric operator.

$$\mathrm{DEV}_{n+1}\left(\mathbf{A}\right) = \mathbf{A}^{\circ} = \mathbf{A} - \frac{1}{3}\,\left(\mathbf{A} : \mathbf{C}_{n+1}\right)\,\mathbf{C}_{n+1}^{-1} \tag{13}$$

In Eq. (13), $\mathbf{A}$ denotes a generic second-order tensor (which in development will assume $\mathbf{S}$ or $\mathbf{H}$). The operator ":" represents the inner product between two second-order tensors, mathematically equivalent to the trace of their product, i.e., $\mathbf{A} : \mathbf{C}_{n+1} = \mathrm{tr}(\mathbf{A}\,\mathbf{C}_{n+1})$.

The deviatoric functions associated with the stiffness model of the system provide a final stress matrix ($\mathbf{S}_{\text{final}}$), shown in Eq. (14). Simo and Hughes (2006) define that $\gamma_\infty = \gamma - 1$, which corresponds to a stiffness portion of the model. Thus, Eq. (14) is rewritten as Eq. (15).

$$\mathbf{S}_{\text{final}} = \gamma_\infty\,\mathbf{S}_{n+1}^{\circ} + \gamma\,\mathbf{H}_{n+1}^{\circ} \tag{14}$$

$$\mathbf{S}_{\text{final}} = (\gamma - 1)\,\mathbf{S}_{n+1}^{\circ} + \gamma\,\mathbf{H}_{n+1}^{\circ} \tag{15}$$

For the final stress expression, as the second Piola-Kirchhoff tensor is not feasible to be compared, a stress transformation is performed, which allows comparing the results. Thus, the Kirchhoff stress tensor (spatial) is calculated through the standard transformation (push-forward), Eq. (16). With the stress already transformed, it is possible to extract numerical data of strain and stress for plotting.

$$\boldsymbol{\sigma}_{n+1} = \mathbf{F}_{n+1}\,\mathbf{S}_{\text{final}}\,\mathbf{F}_{n+1}^{T} \tag{16}$$

To assess the convergence of results, it is necessary to quantify the error. The average error (ϵ) in percentage between the experimental and numerical values is calculated using Eq. (17), being the average of the modules of the relative differences.

$$\epsilon = \frac{1}{n}\sum_{i=1}^{n}\left|\frac{\sigma_{\text{exp}_i} - \sigma_{\text{num}_i}}{\sigma_{\text{exp}_i}}\right| \times 100 \tag{17}$$

With the entire tensorial methodology described, it is also important to highlight the strain energy function (W). This function can be either micromechanical or phenomenological aspects. In the latter case, it is defined for homogeneous and isotropic materials as a function of the strain invariants, $W(I_1, I_2, I_3)$. A further simplification arises when considering incompressible materials, for which the third invariant of the deformation tensor is equal to one. This approach is applicable to various polymeric materials, including polyester. For this particular study, the chosen model is the Modified Yeoh model, Eq. (18), as presented in the

literature (Yeoh, 1993). This model falls under the phenomenological category and has been preferred due to its ability to minimize the average error for polyester fibers, as demonstrated in a similar implementation reported in the literature (da Cruz et al., 2023).

$$W = C_1(I_1 - 3) + C_2(I_1 - 3)^2 + C_3(I_1 - 3)^3 + \frac{C_4}{C_5}\left(1 - \exp\left(-C_5\left(I_1 - 3\right)\right)\right) \tag{18}$$

The model calibration was performed via parametric optimization by minimizing the sum of squared differences between experimental and simulated stresses, evaluated at regular strain intervals during loading and unloading. The objective functional is defined as shown in Eq. (19):

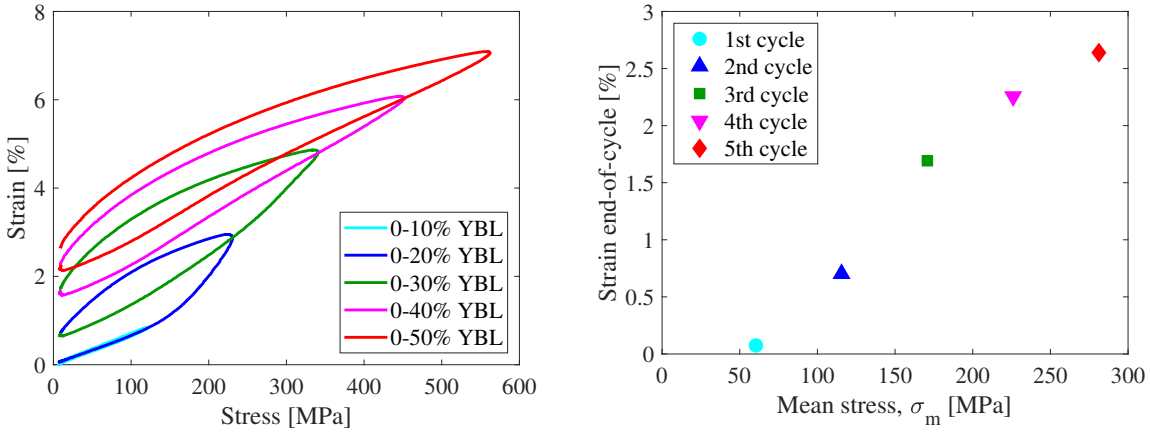
$$\min_{\{C_i,\gamma,\tau\}} J = \sum_{k=1}^{N} \left[\sigma_{\text{exp}}(\varepsilon_k) - \sigma_{\text{num}}(\varepsilon_k; \{C_i, \gamma, \tau\})\right]^2 \tag{19}$$

where σ_{exp} and σ_{num} are the experimental and numerical stresses at strain ε_k, and $\{\gamma, \tau, C_i\}$ are the parameters to be adjusted of the strain energy function and the viscoelastic parameters associated with the internal variable. The optimization was solved under constraints to ensure physical admissibility of parameters, promoting dimensional consistency and best fitting.

3. RESULTS AND DISCUSSION

3.1 Experimental

The main objective of this study concerns the cycle-by-cycle constitutive numerical simulations. However, for reference purposes, it is important to present the experimental stress-strain response, as shown in Fig. 3a.



(a) Stress-strain full-graphs

(b) Strain in the end-of-cycle valley *versus* mean stress

Figure 3: Experimental results.

As shown in Fig. 3a, the first cycle (0 to 10% of the YBL) exhibits an almost linear behavior, with no significant difference between the loading and unloading branches. Another noteworthy observation is the maximum strain of approximately 7% at the peak of the fifth cycle (0 to 50% of the YBL). Additionally, there is a clear trend toward mechanical hysteresis stabilization, as indicated by the progressive reduction in the strain gap between the beginning and end

of each cycle. Figure 3b also shows the strain at the end of the cycle, at zero tension after unloading. Note the stabilization mentioned above with a smaller gap in the difference between deformations between the last cycles.

It is also important to note that the cycle-by-cycle experimental data are used to calibrate the constitutive numerical simulation models. Moreover, the experimental stress values are employed in the calculation of the mean simulation error, as defined in Eq. (17).

3.2 Numerical

For the results of the constitutive numerical simulations, Fig. 4 directly presents the stress-strain response curves obtained through numerical development and optimization.

Visually, the lowest agreement between numerical and experimental data is observed in the 0 to 10% YBL cycle (Fig.4a), whereas the highest visual agreement occurs in the 0 to 50% YBL cycle (Fig.4e).

For all constitutive simulations shown in Fig. 4, when analyzing each cycle individually, a larger error is observed at the last point of the unloading phase. When comparing across cycles, this same error at the end of the unloading phase tends to decrease progressively, likely due to a stabilization, i.e., a reduction in the strain difference between the start and end of each cycle.

Thus, the strong performance of the numerical simulation observed for the dynamic loading cycle from 0 to 50% of the YBL (Fig. 4e) is attributed both to the higher load amplitude applied in this cycle and to the influence of the preceding dynamic history.

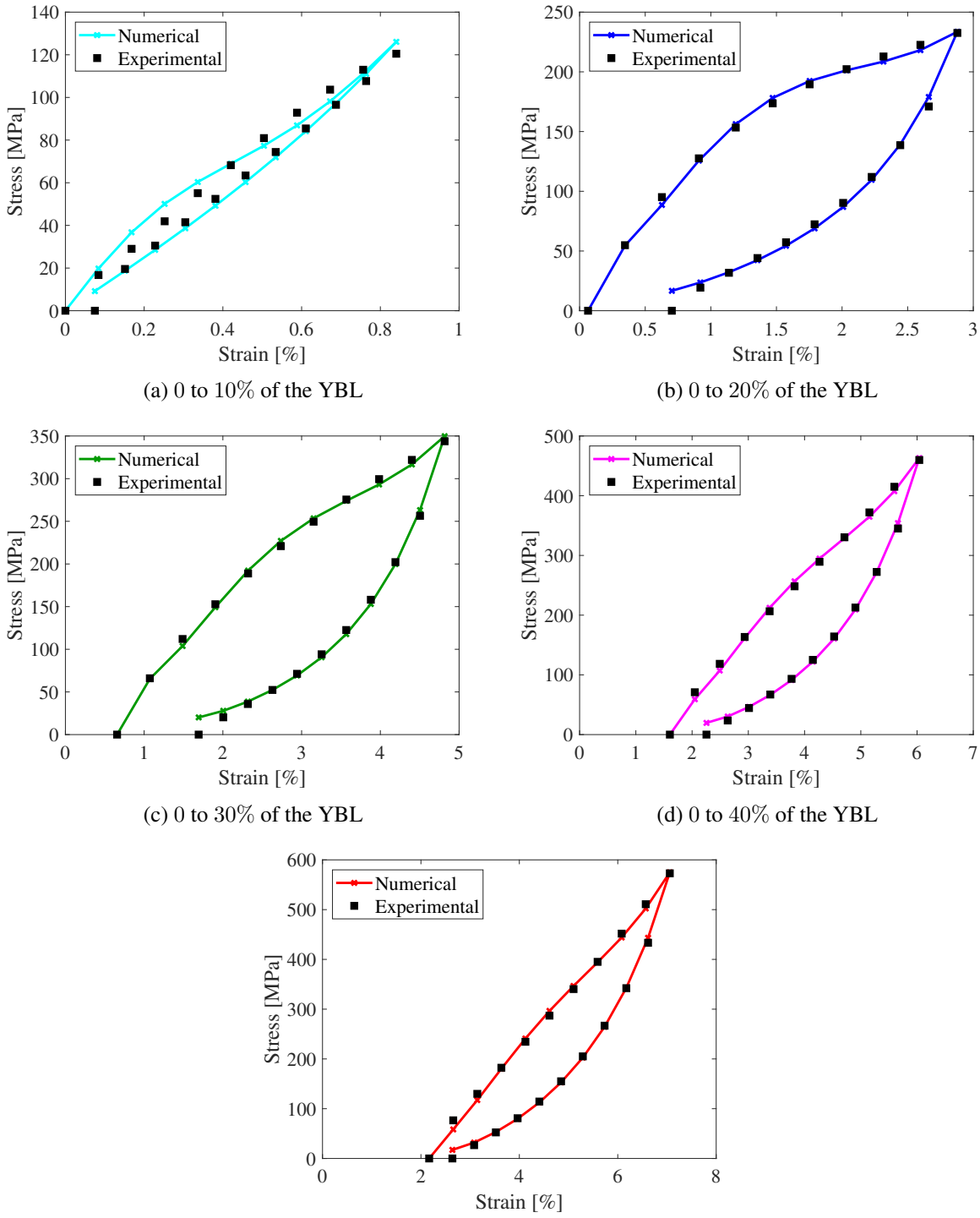
In addition to the visual assessment of the numerical simulation graphs, the mean error (ϵ) is used as a quantitative parameter for each stress-strain simulation, calculated according to Eq. (17). Although this metric does not accurately capture local discrepancies, it provides a global measure of simulation quality, quantitatively representing the agreement between the numerical results and the experimental reference. Table 2 presents the mean error values obtained from the simulations, expressed as percentages.

Table 2: Average error of constitutive numerical simulations, in percentage

	0 to 10%YBL	0 to 20%YBL	0 to 30%YBL	0 to 40%YBL	0 to 50%YBL
ϵ [%]	6.717	3.424	4.297	4.213	3.805

It is noteworthy that, from a purely visual standpoint, the best simulation result appears in the 0 to 50% YBL cycle (Fig.4e), whereas the lowest mean error, according to the quantitative mathematical criterion, is observed in the 0 to 20% YBL cycle (Fig.4b). Both correspond to the lowest mean errors among the numerical simulations. However, this discrepancy may be attributed to the visual perception of the curves: in the higher amplitude cycle (0 to 50% YBL), the similarity between the loading and unloading paths gives the impression of a smaller error; in contrast, the 0 to 20% YBL cycle exhibits more pronounced curvature changes and a clearer distinction between the loading and unloading behavior, which makes the deviation more noticeable despite the smaller numerical error.

Still regarding the mean errors presented in Table 2, it is observed that the values obtained in this study are higher than those reported in the literature. For instance, da Cruz et al. (2023) simulated a stabilized cycle for polyester, specifically the 100th cycle under dynamic loading from 0 to 45% of YBL, and obtained a mean error of 2.2% using the Modified Yeoh model. When compared to the 3.8% obtained in the present study for the 0 to 50% YBL cycle (the closest comparable condition), a higher error is evident. However, this difference



(a) 0 to 10% of the YBL

(b) 0 to 20% of the YBL

(c) 0 to 30% of the YBL

(d) 0 to 40% of the YBL

(e) 0 to 50% of the YBL

Figure 4: Stress-strain graphs for numerical results.

does not undermine the effectiveness of the implemented methodology nor the reliability of the numerical results.

For the numerical simulation results, it is also necessary to extract the values of the constants related to the tensorial formulation (γ and τ) and the Modified Yeoh model (C_n). Table 3 presents these dimensionless phenomenological constants for all simulations.

Table 3: Results of optimized constants in constitutive numerical simulations

	0 to 10%YBL	0 to 20%YBL	0 to 30%YBL	0 to 40%YBL	0 to 50%YBL
γ	0.50	0.50	0.50	0.50	0.50
τ	11.22	22.88	24.06	23.36	23.21
C_1	22.59	7.55	4.74	7.94	9.92
C_2	1.08	0.19	0.10	0.09	0.06
C_3	5.00×10^{-7}	1.30×10^{-7}	0	0	0
C_4	18.26	39.05	29.90	22.79	17.69
C_5	2.87×10^{-4}	6.23	2.14	3.19	4.59

The adopted model is phenomenological, which makes it difficult to assign direct physical or mechanical meaning to its constants. Nevertheless, in addition to being reported for reference, it is worth noting that, with few specific exceptions, all constants associated with the same parameter remain within the same order of magnitude. Furthermore, the value of γ, related to the model's stiffness, remains constant across simulations, an observation also reported in other studies in the literature da Cruz et al. (2023, 2024a,b).

4. CONCLUSION

This study presented a numerical approach to simulate the stress-strain behavior of polyester multifilaments subjected to variable stress dynamic loading cycles, with increasing load amplitudes up to 50% of the Yarn Break Load (YBL). Using a phenomenological hyperelastic model (Modified Yeoh), implemented within a tensor-based formulation grounded in continuum mechanics and calibrated through parametric optimization, the constitutive response was satisfactorily represented across different loading levels.

The results showed that, although the average simulation error varied between cycles, the adopted methodology was able to accurately capture the material's mechanical behavior, even under non-stabilized hysteresis conditions. It was observed that the largest load amplitude (0 to 50% of the YBL) exhibited the smallest visual discrepancy between numerical and experimental data, while the lowest quantitative error occurred in the 0 to 20% cycle, highlighting important nuances between qualitative criteria and global fitting metrics.

Furthermore, the numerical constants associated with the model remained consistent across cycles, reinforcing the robustness of the implemented code. These findings support the viability of the methodology for future applications at higher structural levels, such as strands and sub-ropes, and pave the way for further studies exploring the influence of frequencies, loading rates, and mechanical stabilization effects over multiple cycles. It is also recommended that these tests be replicated for other synthetic fibers, as well for single-cycle loading (without load history).

Acknowledgements

This study was financed in part by the Coordenação de Aperfeiçoamento de Pessoal de Nível Superior – Brazil (CAPES) – Finance Code 001, besides Conselho Nacional de Desenvolvimento Científico e Tecnológico (CNPq), grant number 307889/2022. We would also like to thank Fundação Carlos Chagas Filho de Amparo à Pesquisa do Estado do Rio de Janeiro (FAPERJ), and Fundação de Amparo à Pesquisa do Estado do Rio Grande do Sul (FAPERGS).

REFERENCES

Ahmad, S., Rasheed, A., and Nawab, Y., editors (2020). *Fibers for Technical Textiles*. Topics in Mining, Metallurgy and Materials Engineering (TMMME). Springer Cham.

American Society for Testing and Materials (2018). *Standard Test Methods for Linear Density of Textile Fibers*. American Society for Testing and Materials. ASTM D1577-07(2018).

Banfield, S. and Casey, N. (1998). Evaluation of fibre rope properties for offshore mooring. *Ocean Engineering*, 25(10):861–879.

Bastos, M. B. (2013). Improved high tenacity/high modulus polyester for stiffer mooring ropes. In *2013 MTS/IEEE OCEANS - Bergen*, pages 1–5, Bergen, Norway.

Bastos, M. B. and da Silva, A. L. N. (2020). Evaluating offshore rope fibers: Impact on mooring systems integrity and performance. In *Offshore Technology Conference*, pages OTC–30830–MS, Houston, Texas, USA.

Bastos, M. B., Fernandes, E. B., and da Silva, A. L. N. (2016). Performance fibers for deep water offshore mooring ropes: Evaluation and analysis. In *OCEANS 2016 - Shanghai*, Shanghai, China.

Bhat, G., editor (2017). *Structure and Properties of High-Performance Fibers*. Woodhead Publishing Series in Textiles. Woodhead Publishing.

da Cruz, D. M. (2022). Estudo teórico, experimental e numérico do comportamento viscoelástico e caracterização de fibras sintéticas poliméricas. Trabalho de Conclusão de Curso (Graduação em Engenharia Mecânica), Universidade Federal do Rio Grande, Escola de Engenharia, Rio Grande/RS, Brasil.

da Cruz, D. M., Popiolek Júnior, T. L., Barreto, M. A., de Souza, S. P., Zangalli, L. B., da Cruz Júnior, A. J., Martins, T. C., da Silva, A. L. N., Bastos, I. N., and Guilherme, C. E. M. (2024a). Numerical simulation with hyperelastic constitutive model for high-performance multifilaments used in offshore mooring ropes. *The Journal of Engineering and Exact Sciences*, 10(2):17255.

da Cruz, D. M., Popiolek Júnior, T. L., Barreto, M. A., Guilherme, C. E. M., and Stumpf, F. T. (2023). Evaluation of energy models for numerical simulation of the mechanical behavior of polyester multifilaments. *The Journal of Engineering and Exact Sciences*, 9(1):15321–01e.

da Cruz, D. M., Stumpf, F. T., Vassoler, J. M., and Guilherme, C. E. M. (2025). Assessment of the effects of uv-a exposure on the mechanical strength of offshore mooring multifilaments. *Acta Polytechnica*, 64(6):487–500.

da Cruz, D. M., Zangalli, L. B., Barreto, M. A., Bastos, I. N., and da Silva, A. L. N. (2024b). Numerical simulation of the stress-strain behavior of polyester subropes for offshore mooring and relationship with change stiffness during the test protocol. In *ROG.e 2024*, page 3215, Rio de Janeiro, Brasil.

da Cruz, D. M., Zangalli, L. B., Barreto, M. A., da Silva, A. L. N., and Bastos, I. N. (2024c). Offshore mooring challenges for FOWT systems and MRE devices: Synthetic fiber solutions for mooring ropes. In *ROG.e 2024*, page 3210, Rio de Janeiro, Brasil.

Del Vecchio, C. J. M. (1992). *Light weight materials for deep water moorings*. PhD thesis, University of Reading, Reading, UK.

Flory, P. J. (1961). Thermodynamic relations for high elastic materials. *Transactions of the Faraday Society*, 57:829–838.

International Organization for Standardization (2005). *Textiles — Standard atmospheres for conditioning and testing*. International Organization for Standardization. ISO 139:2005.

International Organization for Standardization (2009). *Textiles — Yarns from packages — Determination of single-end breaking force and elongation at break using constant rate of extension (CRE) tester*. International Organization for Standardization. ISO 2062:2009.

International Organization for Standardization (2019). *Fibre ropes for offshore stationkeeping — Part 2: Polyester*. International Organization for Standardization. ISO 18692-2:2019.

Lee, M.-Y., Flory, J., and Yam, R. (1999). Abs guide for synthetic ropes in offshore mooring applications. In *Offshore Technology Conference*, pages OTC–10910–MS, Houston, Texas, USA.

Simo, J. C. and Hughes, T. J. R. (2006). *Computational Inelasticity*. Interdisciplinary Applied Mathematics. Springer Science & Business Media, New York, 7 edition.

Stumpf, F. T., de Ávila Barreto, M., da Cruz, D. M., and Guilherme, C. E. M. (2024). Numerical simulation of multi-material hybrid lines for offshore mooring. *Ocean Engineering*, 305:117979.

Stumpf, F. T., Guilherme, C. E. M., da Cruz, D. M., da Fonseca Thomé da Silva, A. H. M., and Bastos, M. B. (2023). A general constitutive model for the numerical simulation of different synthetic fibres used in offshore mooring. *Ships and Offshore Structures*, 18(9):1338–1344.

Weller, S. D., Johanning, L., Davies, P., and Banfield, S. J. (2015). Synthetic mooring ropes for marine renewable energy applications. *Renewable Energy*, 83:1268–1278.

Yeoh, O. H. (1993). Some forms of the strain energy function for rubber. *Rubber Chemistry and Technology*, 66(5):754–771.